PHOTONICS Research

Structured vortices generated by metasurface holography

Zhen Mou,[1] Changda Zhou,[1] Peiyao Lu,[1] Qingyang Yue,[1] Shuyun Wang,[1,2] and Shuyun Teng[1,*]

[1]Shandong Provincial Key Laboratory of Optics and Photonic Device & School of Physics and Electronics, Shandong Normal University, Jinan 250014, China
[2]e-mail: wangshuyun65@163.com
*Corresponding author: tengshuyun@sdnu.edu.cn

Received 14 April 2021; revised 4 August 2021; accepted 20 August 2021; posted 24 August 2021 (Doc. ID 427745); published 30 September 2021

Highly customized and miniaturized structured light is expected in many application fields. A kind of structured vortex generators is proposed based on a metasurface consisting of rectangular nanoholes etched in a silver film, and the generated vortices with the same or different topological charges are distributed along the radial direction. The geometric metasurface is completed with the help of optical holography technology, and the structured vortex generator possesses high working efficiency and large information capacity. The proposed vortex generators work under circularly polarized light illumination, and the reproduced vortices of multiplexing vortex generator depend on the handedness of the circularly polarized light. This work paves a way to generate new structured light fields. The radially distributed vortices may be utilized to simultaneously screen or separate microparticles. The compact design of the structured vortex generator and the convenient switch of different structured vortices will be a benefit to expand the applications of structured vortex fields.

https://doi.org/10.1364/PRJ.427745

1. INTRODUCTION

The optical vortex with nonuniform phase distribution and phase singularity has been an ongoing subject of concern in the past 30 years [1,2]. One typical vortex usually behaves as a helical phase wavefront and an annular intensity cross section [3,4]. One complex structured vortex, like the Laguerre–Gaussian (LG) beam [5], the Bessel–Gaussian (BG) beam [6], or the Mathieu beam [7], behaves with multiple-ring or multiple-spot intensity distribution, and the topological charges of the spiral phases in different regions may be same or different [8,9]. Because the vortex beam carries the orbital angular momentum, which provides the interaction of light and matter, it can be widely applied in optical tweezers [10], optical trapping [11], quantum communication [12], and quantum information processing [13]. The structured vortex with custom intensity and spiral phase distribution may expand to the wide applications in fields like 3D spiral fabrication [14,15].

A vortex beam may be generated by using many methods, such as the beam interference [16], forked grating [3], spatial light modulator [17], spiral slit [18,19], spiral phase plate [20], and metasurface [21,22]. In comparison with the other methods, metasurfaces can cause spatially varying optical responses through the interaction between the light field and nanostructure instead of spatial accumulation effect along an optical path [23]. Therefore, metasurfaces show the advantages of compact structure and powerful light manipulation and have attracted great interest. Flat optical devices, including metamirrors [24], metalenses [25,26], meta-axicons [27], metafilters [28], and metaholograms [29,30], have been proposed.

With the help of optical holography technology, metasurface holography can realize the record of the amplitude and phase of any object and the reproduction of the object using the metahologram [31–34]. Recently, some groups have reported the reproduction of designated intensity distribution or shaped wavefront. Ni *et al.* reproduced the word "PURDUE" as the test virtual object through designing the metahologram composed of V-shaped holes [35]. Dolev *et al.* performed the beam shaping through designing the amplitude holographic grating and obtained a vortex beam and an Airy beam [36]. Mueller *et al.* designed a chiral metahologram consisting of elliptical pillars and reproduced different images of cartoon pet patterns with the control of circularly polarized light [37]. These works show the performance of metaholograms with low noise, high resolution, and tunability, which will open more opportunities in the applications of high-capacity optical imaging and information processing.

Besides the intensity modulation, wavefront shaping, and multiplexing image reproduction, as we know, the powerful light manipulation ability of metasurface holography is far more than above [38,39]. In this paper, we utilize metasurface holography to reproduce simultaneously the intensity pattern and phase distribution. We design a kind of structured vortex

generator (SVG) using the designed metaholograms and obtain the structured vortices with multiple-ring intensity and a spiral phase. The topological charges of spiral phases in different radial regions may be same or different. The proposed SVG consists of rectangular holes etched in silver film. The structure information of SVG comes from a Fresnel hologram of the structured vortex field. Besides this fundamental design, the multiplexing metasurface SVG is also proposed to output the polarization controllable structured vortex. The reproduced results of structured vortices show our designed SVGs have low noise, high working efficiency, and large information capacity. The generation of a structured vortex and the design of a metasurface SVG will promote the applications of the metasurface holography and structured vortices in the fields of optical manipulation and integrated optics.

2. DESIGN PRINCIPLE

The structured vortex has the spatial distribution of multiple-ring intensity and a spiral wavefront. Two parameters of n and m_i are used to describe this structured light field, where the parameter n takes a nonnegative integer and reflects the number of radial nodes among the intensity distribution, The parameter m_i takes any integer with the subscript of i, taking the value of $0, 1, \ldots, n$. The value of m_i represents the topological charge of the vortex, and it means the light field in the ith radial region has an azimuthal phase change of $2m_i\pi$. Certainly, the value of m_i in different radial regions may be equal or different. Figure 1(a) shows the intensity and phase distributions of one structured vortex field with $n = 1$ and $m_0 = m_1 = 2$. Obviously, the number of bright rings is one more than the value of n. The phase changes twice that of 2π along the counterclockwise direction, and the initial phases of vortices at different regions are different. This case is just like the distribution rule of an LG beam.

In order to generate this kind of structured vortex field using a metasurface, we construct the metahologram according to the Fresnel holography technique [40]. The structure information of the metahologram comes from the Fresnel transformation of the structured vortex field. Thus, we first construct the complex amplitude of the structured vortex field, which can be denoted by $U_0(x, y)$ (see Appendix A). Then, we obtain the Fresnel holography diagram through the Fresnel transformation. This process can be expressed by

$$U_H(x, y) = U_0(x, y) * \left\{ \frac{\exp(jkd)}{j\lambda d} \exp\left[\frac{jk}{2d}(x^2 + y^2) \right] \right\}, \quad (1)$$

where $U_H(x, y)$ is the spatial distribution on the hologram, d is the diffraction distance, and $k = 2\pi/\lambda$ is the wave vector with the incident wavelength of λ. The symbol * represents the convolution operation.

In order to simplify the coding capacity of the Fresnel hologram, we set one or more threshold values according to the amplitude information, like the case of Fig. 1(b), where Holo and T-Holo denote the phase holograms without and with setting a threshold value, respectively. We can see that the spatial region of phase distribution gets smaller after setting a threshold value, which is more convenient for the design of the metasurface. In practice, we utilize the discrete rectangular nanoholes to construct the metahologram. The amplitudes and phases of the metahologram correspond to the data for the Fresnel hologram of $U_H(x, y)$. Thus, the expression of $U_H(x, y)$ should be discretized and the above equation can be substituted by the following form:

$$U_H(p\delta_x, q\delta_y) = U_0(p\delta_x, q\delta_y) * \left\{ \frac{\exp(jkd)}{j\lambda d} \exp\left[\frac{jk}{2d}(p^2\delta_x^2 + q^2\delta_y^2) \right] \right\}, \quad (2)$$

where the parameters of p and q take integers, and δ_x and δ_y represent the sampling intervals of the metasurface along two orthogonal directions. $p\delta_x$ and $q\delta_y$ determine the positions of the sampling points along two directions, which correspond to the spatial coordinates of nanoholes on the metasurface. The phase information of the metahologram can be incarnated with the help of the rotation of the rectangular nanohole because the rotated nanohole may introduce a geometric phase delay. Certainly, the introduced phase delay appears among the cross-polarization, and it equals twice the rotation angle [41,42]; Fig. 1(c) shows the 2-times relation between the phase delay and the rotation angle of the nanohole.

If one performs the inverse Fresnel transformation of $U_H(x, y)$ or $U_H(p\delta, q\delta_y)$, one can obtain the image of the designated vortex field of $U_0(x, y)$ through the expression of the reproduced vortex field; the case of Eq. (1) or Eq. (2) illustrates the difference of one complex constant. Through above operation, one metasurface SVG is formed by using the rotated rectangular nanoholes, and the structured vortex field can be reproduced under the circularly polarized light illumination. The reproduced image of the structured vortex field appears at the propagation distance of d because the inverse Fresnel transformation of the metahologram is done. Figure 1(d) shows the schematic diagram for the generation of structured vortex field based on the designed metasurface. The inserted diagram on the bottom of Fig. 1(d) is the magnified structure of the metasurface.

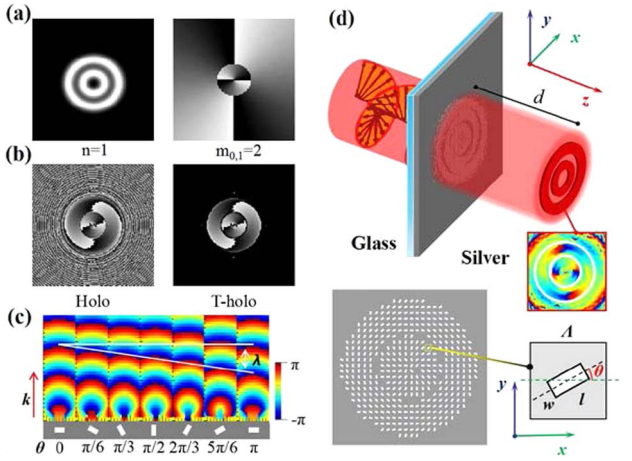

Fig. 1. (a) Number of outer loops by n as 1 and the spiral phase wavefront determined by $m_{0,1}$ as 2; (b) phase information of the structured light beams with hologram (Holo) and thresholding hologram (T-holo); (c) relation between the phase delay φ and the rotation angle θ of hole; and (d) schematic diagram of the metasurface holography under circularly polarized light illumination.

3. NUMERICAL SIMULATIONS

In order to increase optical performance of the designed SVG, we first optimize the parameters of the metasurface and ascertain the condition for the maximum transmittance of metasurface through the simulation calculations (see Appendix B). The thickness of the silver film deposited on the glass substrate takes 150 nm, and the length and width of the rectangular hole take $l = 135$ nm and $w = 70$ nm. The intervals of two adjacent nanoholes along two orthogonal directions take $\Lambda = 250$ nm. Theoretically, we can design any SVG on the basis of the above theoretical analysis. Here, three kinds of SVGs are provided. The first one is the SVG that generates a radially structured vortex carrying the same topological charge; the second one is the SVG that forms a radially structured vortex carrying different topological charges; and the third one is the multiplexing SVG with the structured vortex changing with the handedness of the incident circular polarization.

A. SVG Carrying the Same Topological Charge

This kind of SVG can generate the structured vortex fields where the topological charge of the vortex distributed in different radial regions is same. The gray-scale patterns at the left of Figs. 2(a) and 2(b) give the phase distributions of this kind of structured vortex; the parameter of n equals 0 and 2, and the parameter of m takes 2 for two cases, where the inserted patterns on the lower right corners of Figs. 2(a) and 2(b) are the intensity distributions. Obviously, the number of bright rings among the intensity distribution is one more than the value of n. The value of the parameter of m corresponds to the topological charge of the vortex in each radial region. It is easy to see that this structured vortex light is like the LG light [5].

In the designed structured vortex field, we perform a Fresnel transformation according to Eq. (1) and construct the corresponding metahologram according to the discretized data of Eq. (2). Then the reproduced image of the structured vortex field can be obtained with the right-handed circularly polarized light illumination. The color patterns at the right of Figs. 2(a) and 2(b) give the simulation results for the intensity and phase distributions of the reproduced light fields. In these two designs, the distance between the metasurface and the observation plane is set as $d = 10$ μm. For convenient observation of the phase change, some curves with arrows are inserted in the patterns of phase distributions. By comparing Figs. 2(a) and 2(b), we can see that the intensity and phase distributions for the reproduced fields are almost the same as the designed fields. The clear boundaries between different characteristic regions indicate that the designed holography metasurfaces for the SVGs have higher resolution and precision.

B. SVG Carrying Different Topological Charges

The optical vortex of the structured vortex field at different radial regions may have different topological charges. The second kind of SVG can generate this structured vortex field. The intensity and phase distribution characteristics of this kind of structured vortex can be seen from the patterns at the left of Figs. 2(c) and 2(d), where the parameter of n equals 2. The parameter of m_i takes 1, 2, and 3 for Fig. 2(c) and 1, −2, and 3 for Fig. 2(d). One can see the phases in the inner regions of the two patterns increase 2π in counterclockwise direction, and the phases in the outer regions of the two patterns increase three times 2π in counterclockwise direction. In the middle regions for the two cases, the phases increase two times 2π along counterclockwise direction and clockwise direction, respectively. The inserted intensity distributions in the lower right corners of Figs. 2(c) and 2(d) show three bright rings appear; they are one more than the value of n.

For these structured vortex fields, we perform the above-mentioned operation process and obtain their Fresnel metaholograms. We also set the distance between the metasurface and the observation plane at $d = 10$ μm and simulate the Fresnel diffraction of the metahologram. The images of the structured vortex fields are reproduced, as shown in the color patterns on the right of Figs. 2(c) and 2(d). One can easily see that the phases in the radial regions from inside to outside change once, twice, and three times 2π. The increase directions of phases at the middle regions for the two cases are opposite. The inserted intensity patterns at the lower right of Figs. 2(c) and 2(d) are also the same as the designed ones. Three bright rings appear in any case.

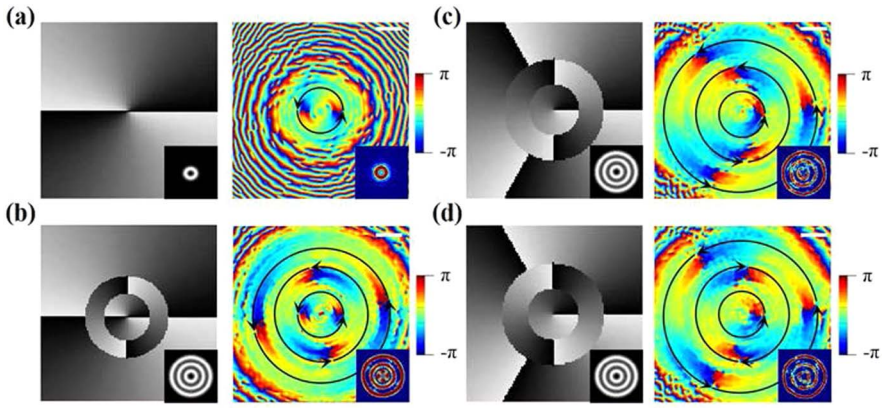

Fig. 2. Intensity and phase distributions of the designed structured fields and the reproduced structured fields, where (a) the parameter of n takes 0 and the parameter of m_0 takes 2; (b) the parameter of n takes 2 and the parameter of m_i takes $m_0 = m_1 = 2$; and the parameter of n takes 2 and the parameter of m_i takes (c) $m_0 = 1$, $m_1 = 2$, and $m_2 = 3$ and (d) $m_0 = 1$, $m_1 = -2$, and $m_2 = 3$ (white bar, 6 μm).

C. Multiplexing SVG with Polarization Dependence

We also design a polarization-dependent SVG that can generate the different structured vortices with the illumination of the left-handed circularly polarized (LCP) light and right-handed circularly polarized (RCP) light. In order to realize the polarization control of the structured vortex field, we design one polarization multiplexing metasurface. We first obtain the Fresnel transformation of two structured vortex fields, as in the above operation. Then, we compare the amplitude information of the two Fresnel fields and construct one compound Fresnel field keeping only the information of the field with the greater amplitude. Setting a threshold value and rotating the rectangular nanoholes, the polarization multiplexing metasurface is formed.

Figures 3(a) and 3(c) give the combinations of the multiplexing structured vortex field, which includes two different structured vortex fields. One is the structured vortex field with the parameters of $n = 0$ and $m_0 = 2$, and the other is the structured vortex field with the parameters of $n = 1$, $m_0 = 1$, and $m_1 = -2$. The gray-scale patterns of Figs. 3(a) and 3(c) show the intensity and phase distributions of two structured vortex fields. For the former, there is one bright ring and the phase changes two times 2π along the counterclockwise direction. For the latter, there are two bright rings, and the inner phase changes 2π along the counterclockwise direction, and the outer phase changes two times 2π along the clockwise direction.

The color patterns of Figs. 3(b) and 3(d) show the intensity and phase distributions of the reproduced structured vortex fields generated by the same metahologram with the LCP and RCP light illumination. From the simulation results, we can see one bright ring appears with the RCP light illumination, and two bright rings are produced with the LCP light illumination. The phase for the former changes two times 2π along the counterclockwise direction. For the latter, the inner phase changes 2π along the counterclockwise direction, and the outer phase changes two times 2π along the opposite direction. Obviously, the reproduced vortex fields are the same as the designed ones.

It is interesting that the phase distribution with the opposite topological charge appears when the designed SVG is illuminated by the orthogonal circularly polarized light. As shown in the dark areas in Figs. 3(b) and 3(d), although the intensity of the bright ring disappears under the orthogonal circularly polarized light illumination, the phase changing in the opposite direction can still be seen. We think this is because the SVG is designed on the basis of the geometric phase which is being carried by the cross polarization, and the designed SVG is similar to the spiral phase plate.

Similarly, any structured light field can be generated by building the model of the structured light field and constructing the appropriate metahologram, although only three kinds of SVGs are provided in this paper. Furthermore, it needs to be pointed out that the determination of metasurface parameters, the realization of the metahologram, the simulations for the wavefront of single rectangular nanohole, and the reproduction of the metahologram are completed by using the finite-difference time-domain technique (see Appendix C).

4. EXPERIMENT MEASUREMENT

A practical experiment is performed to verify the performance of our proposed metasurface SVG. We manufacture one sample of the polarization-dependent SVG; Fig. 4(b) gives the scanning electron microscope (SEM) image and a part of its magnified image. During the manufacture of the sample, a silver film with the thickness of 150 nm is deposited on the glass substrate by using the magnetron sputtering method, and the rectangular nanoholes are fabricated by means of the focused ion beam etching method. We put the sample of SVG into the optical path shown in Fig. 4(a) and measure its reproduced image. The linearly polarized light emitted from the He–Ne laser changes into the RCP and LCP light with the help of a polaroid (P_1) and a quarter-wave plate (QWP_1). Then, it illuminates the sample from the glass substrate, and one microscope objective (MO_1) magnifies the transmission intensity distribution of the sample. A polaroid (P_2) and a quarter-wave plate (QWP_2) are used to reduce background light. The magnified intensity distribution is received by a two-dimensional CCD. Figures 4(c) and 4(d) give the measured results for the intensity distributions of the diffraction fields with different

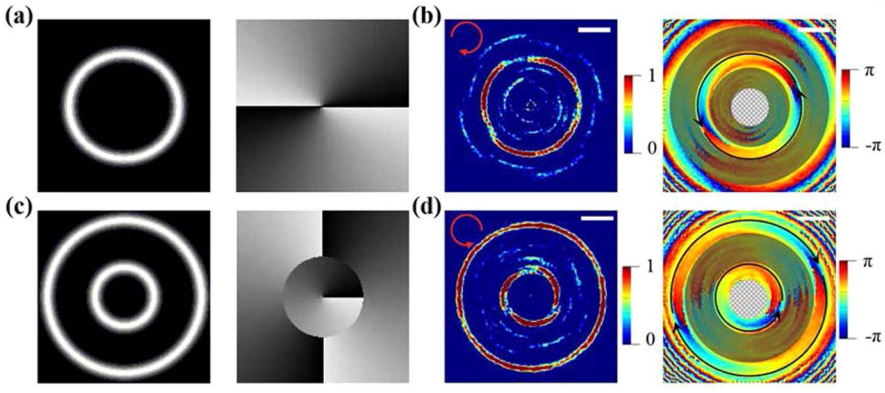

Fig. 3. Intensity and phase distributions of (a), (c) the designed structured vortex fields and (b), (d) the reproduced structured lights with different polarization light illuminations, where the parameter of n takes 0 and the parameter of m_0 takes 2 for (a) and (b), and the parameter of n takes 1 and the parameter of $m_0 = 1$ and $m_1 = -2$ for (c) and (d) (white scale bar, 6 μm).

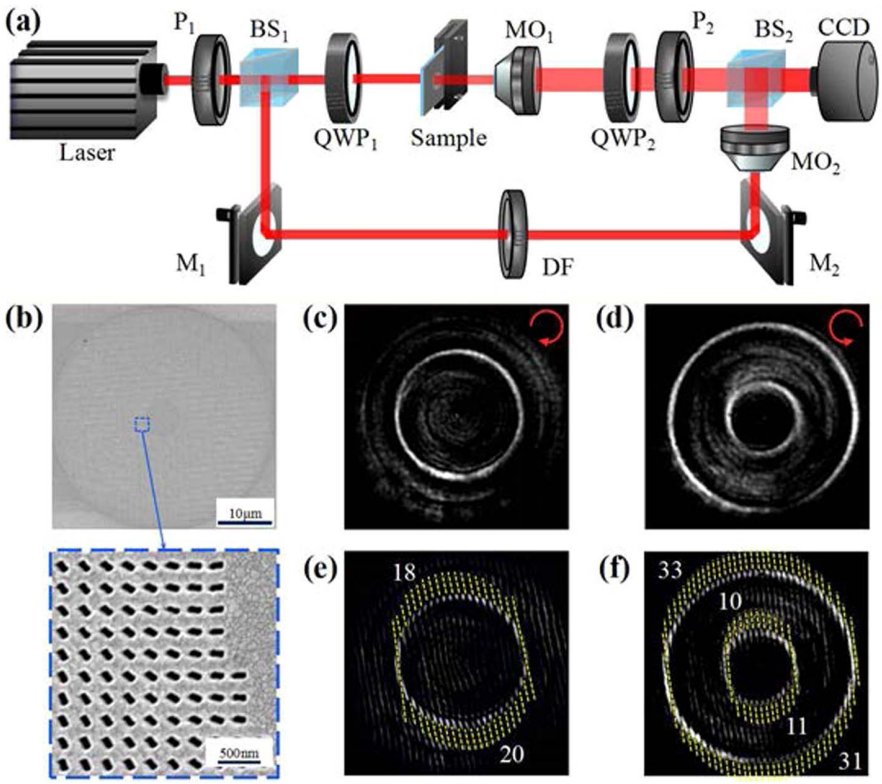

Fig. 4. (a) Experiment setup for measuring the diffraction intensity and phase distributions of the SVG sample; (b) SEM image of the SVG sample, where the inserted patterns at the bottom are the magnified part; (c) and (d) the measured diffraction intensity distributions under RCP and LCP light illumination; and (e) and (f) the interference results of the reproduced vortex fields and the plane wave for two illumination conditions, where the wavelength of the illuminating light takes 632.8 nm.

polarized light illuminations. In order to measure the phase distribution of the structured vortex field, we add a reference light path to realize the interference of one plane wave and the structured vortex field. The beam splitters (BS_1 and BS_2) split the light beam and combine light beams, and the dense filter (DF) controls the intensity of the reference light. Figures 4(e) and 4(f) give the measured interference results under the two illumination conditions.

From Figs. 4(c) and 4(d), one can see that one bright ring appears with the RCP light illumination and two bright rings appear with the LCP light illumination. These are the same as the simulated results of Figs. 3(b) and 3(d). From the interference results in Figs. 4(e) and 4(f), one can observe many bright spots with respect to the positions of the bright rings. For convenient comparison, we label their positions near these bright spots by the short dashed lines. The numbers of the bright spots for two symmetric parts of any ring are also marked out. It is easy to see that the difference of bright spots at two symmetric parts in Fig. 4(e) is 2, which corresponds to the value of the parameter of m. Similarly, From Fig. 4(f), one can see that the difference of bright spots at two symmetric parts is 1 for the inner ring and 2 for the outer ring. Moreover, comparing the numbers of bright spots at two symmetric parts located on the inner and outer rings, we can find for the inner case, the number at the top is smaller than the one at the bottom, but for the outer case, the number at the top is larger than the one at the bottom. This indicates that the topological charge of the inner vortex has the opposite sign in comparison with that of the outer vortex. These are just with respect to our designed values of 1 and −2. Obviously, all these measured results are consistent with the theoretical and simulated results. These results also verify that our proposed SVGs have reliable performance.

5. CONCLUSIONS

In summary, we designed metasurface SVGs on the basis of metasurface holography. Our proposed metasurface SVGs consist of rectangular nanoholes, and they modulate the amplitude and phase of light fields to generate the structured vortex lights. Three kinds of metasurface SVGs are created: an SVG with the same topological charge, an SVG with different topological charges, and a polarization multiplexing SVG. The simulation and experiment results show the reproduced images of the structured vortex fields can appear as expected. The generation of the structured vortices can realize the parallel output of several vortices, which can be applied in optical manipulation, including particle screening and trapping with many channels, and the polarization multiplexing SVG can also be utilized with flexible control. The advantages of the metasurface, including the ultrathin structure, flexible control, large information capacity, and easy integration, offer the proposed SVGs more potential applications, from high-resolution imaging and micromanipulation to quantum communication.

APPENDIX A: MODEL OF STRUCTURED VORTEX

One structured vortex field $U_0(x,y)$ points to a combination of the fields carrying spiral phase and annular intensity, and it can be expressed in the following form:

$$U_0(x,y) = \sum_{i=0}^{n} C_i \exp\left\{-\frac{[(x^2+y^2)^{1/2} - R_i]^2}{w_{0i}^2}\right\} \exp(jm_i\phi), \tag{A1}$$

where C_i is the amplitude of the light field, R_i is the center position of the radius of the bright ring, w_{0i} represents the width of the bright ring, and $\exp(jm_i\phi)$ denotes the spiral phase. Therefore, the structured vortex has the spatial distribution of multiple-ring intensity and a spiral wavefront.

The amplitude and phase information can be recorded based on optical holography technology, and the image of the object can be reproduced under the reference light illumination. After ascertaining the parameters of the structured vortex, we perform the Fresnel transformation, and the transformed field can be written as Eq. (1). Through the inverse Fresnel transformation, one can obtain the optical field at the propagation distance of d,

$$U_R(x_r,y_r) = \left(\frac{1}{\lambda d}\right)^2 U_0(x_r,y_r). \tag{A2}$$

Obviously, it is just the target function of $U_0(x,y)$. This is the physical mechanism of Fresnel holography and reproduction.

APPENDIX B: OPTIMIZATION OF METASURFACE

The sampling interval or the information content is the key issue for image reproduction. In terms of the Nyquist sampling theorem, when the propagation distance d is set at 10 μm, the maximum sampling interval is ascertained as $(\lambda d/N)^{1/2} = 250$ nm with $\lambda = 632.8$ nm and $N = 100$. We choose the sampling interval as 250 nm. Then, the transmission intensity needs to be set with a value as large as possible. The transmission intensity of the rectangular nanohole varies with its length and width. According to the simulation results, we can ascertain the length and width of the rectangular hole, using 135 nm and 70 nm so as to obtain the maximum transmission intensity.

While the incident light takes the RCP, the transmitted polarization state of nanohole in the circular base can be expressed by [41,42]

$$t_c = \frac{A}{2}\begin{pmatrix}0\\1\end{pmatrix} + \frac{B}{2}e^{-j2\alpha}\begin{pmatrix}1\\0\end{pmatrix}, \tag{B1}$$

where $A = a_x + a_y e^{j\delta}$ and $B = a_x - a_y e^{j\delta}$, a_x and a_y are the amplitudes of transmission field along the two major axes, δ is the phase delay of two field components along the two major axes, and α is the direction angle of the fast axis with respect to the x axis. The first term also takes the RCP; the second term is the LCP. Here, we just use the additional phase of $\exp(-j2\alpha)$ among the cross-polarization conversion to construct the metahologram. Certainly, the first term is the unexpected component, and the effective contribution is proportional to the ratio of B/A. Under the given condition, the optimized result shows that B/A reaches about 0.82.

Though the polarization conversion efficiency of this nanohole is not too high, the parameters for the rectangular hole are the optimization results after considering comprehensively the transmission intensity, the sampling points, and the polarization conversion.

APPENDIX C: SIMULATION METHOD

The realization of the metahologram, the determination of metasurface parameters, and the simulated diffraction distributions are obtained by using the finite-difference time-domain technique. In practical simulation calculations, the perfectly matched layers are used as the boundaries to prevent nonphysical scattering; the minimum mesh step is set at 2 nm. The RCP light is chosen as the illuminating light for the results in Figs. 1 and 2, and the RCP and LCP lights are chosen as the illuminating lights for the results in Fig. 3. The dielectric constant of silver for the wavelength of 632.8 nm is taken as the value given by Palik [43].

During the determination of the metasurface parameters, the calculation conditions are chosen as the detection plane at 2 μm away from the nanohole etched on the silver film, with the length and width of the rectangular nanohole swept from 0 to 150 nm, with a step of 5 nm. For realization of the metahologram, the positions of nanoholes are located on the sampling points of the Fresnel hologram. The construction of the metahologram model is finished according to the written script and the default parameters.

We set the corresponding parameters of the calculation phenomenon, including the thickness of the silver film, the length and width of the nanohole, the intervals of two adjacent nanoholes along two orthogonal directions, the rotation angle of the nanohole at any point, the illumination condition, and the monitor plane of the reproduced image. Thus, the intensity and phase distributions are calculated based on the iteration rule of electromagnetic fields. Many simulated calculations with respect to different metaholograms provide the solid foundation for the design of the practical metaholograms.

Funding. Natural Science Foundation of Shandong Province (ZR2020KA009); National Natural Science Foundation of China (10874105).

Disclosures. The authors declare no conflicts of interest.

REFERENCES

1. P. Coullet, L. Gil, and F. Rocca, "Optical vortices," Opt. Commun. **73**, 403–408 (1989).
2. Y. Shen, X. Wang, Z. Xie, C. Min, and X. Yuan, "Optical vortices 30 years on: OAM manipulation from topological charge to multiple singularities," Light Sci. Appl. **8**, 90 (2019).
3. M. Padgett, J. Courtial, and L. Allen, "Light's orbital angular momentum," Phys. Today **57**, 35–40 (2004).
4. X. Cai, J. Wang, M. J. Strain, B. Johnson-Morris, J. Zhu, M. Sorel, J. L. O'Brien, M. G. Thompson, and S. Yu, "Integrated compact optical vortex beam emitters," Science **338**, 363–366 (2012).
5. S. Haddadi, O. Bouzid, M. Fromager, K. Hasnaoui, A. Harfouche, E. Cagniot, A. Forbes, and K. Ait-Ameur, "Structured Laguerre-Gaussian

beams for mitigation of spherical aberration in tightly focused regimes," J. Opt. **20**, 045602 (2018).
6. K. Zhu, G. Zhou, X. Li, X. Zheng, and H. Tang, "Propagation of Bessel-Gaussian beams with optical vortices in turbulent atmosphere," Opt. Express **16**, 21315–21320 (2008).
7. Y. Zhang, X. Yang, and J. Gao, "Generation of nondiffracting vector beams with ring-shaped plasmonic metasurfaces," Phys. Rev. Appl. **11**, 064059 (2019).
8. Y. Yang, G. Thirunavukkarasu, M. Babiker, and J. Yuan, "Orbital-angular-momentum mode selection by rotationally symmetric superposition of chiral states with application to electron vortex beams," Phys. Rev. Lett. **119**, 094802 (2017).
9. S. Mei, M. Q. Mehmood, S. Hussain, K. Huang, X. Ling, S. Y. Siew, H. Liu, J. Teng, A. Danner, and C. W. Qiu, "Flat helical nanosieves," Adv. Funct. Mater. **26**, 5255–5262 (2016).
10. D. G. Grier, "A revolution in optical manipulation," Nature **424**, 810–816 (2003).
11. C. Liberale, P. Minzioni, F. Bragheri, F. De Angelis, E. Di Fabrizio, and I. Cristiani, "Miniaturized all-fibre probe for three-dimensional optical trapping and manipulation," Nat. Photonics **1**, 723–727 (2007).
12. M. Mirhosseini, O. S. Magaa-Loaiza, M. N. O'Sullivan, B. Rodenburg, M. Malik, M. P. J. Lavery, M. J. Padgett, D. J. Gauthier, and R. W. Boyd, "High-dimensional quantum cryptography with twisted light," New J. Phys. **17**, 033033 (2014).
13. Z. Q. Zhou, Y. L. Hua, X. Liu, G. Chen, J. S. Xu, Y. J. Han, C. F. Li, and G. C. Guo, "Quantum storage of three-dimensional orbital-angular-momentum entanglement in a crystal," Phys. Rev. Lett. **115**, 070502 (2014).
14. J. Ni, Y. Hu, S. Liu, Z. Lao, S. Ji, D. Pan, C. Zhang, B. Xu, J. Li, D. Wu, and J. Chu, "Controllable double-helical microstructures by photonic orbital angular momentum for chiroptical response," Opt. Lett. **46**, 1401–1404 (2021).
15. J. Ni, C. Wang, C. Zhang, Y. Hu, L. Yang, Z. Lao, B. Xu, J. Li, D. Wu, and J. Chu, "Three-dimensional chiral microstructures fabricated by structured optical vortices in isotropic material," Light Sci. Appl. **6**, e17011 (2017).
16. A. Kapoor, M. Kumar, P. Senthilkumaran, and J. Joseph, "Optical vortex array in spatially varying lattice," Opt. Commun. **365**, 99–102 (2016).
17. Y. Ohtake, T. Ando, N. Fukuchi, N. Matsumoto, and T. Hara, "Universal generation of higher-order multiringed Laguerre-Gaussian beams by using a spatial light modulator," Opt. Lett. **32**, 1411–1413 (2007).
18. H. Wang, L. Liu, C. Zhou, J. Xu, M. Zhang, S. Teng, and Y. Cai, "Vortex beam generation with variable topological charge based on a spiral slit," Nanophotonics **8**, 317–324 (2019).
19. C. Zhou, M. Zhen, Z. Li, and S. Teng, "Compound plasmonic vortex generation based on spiral nanoslits," Front. Phys. **16**, 33503 (2021).
20. M. W. Beijersbergen, R. P. C. Coerwinkel, M. Kristensen, and J. P. Woerdman, "Helical-wavefront laser beams produced with a spiral phase plate," Opt. Commun. **112**, 321–327 (1994).
21. E. Karimi, S. A. Schulz, I. De Leon, H. Qassim, J. Upham, and R. W. Boyd, "Generating optical orbital angular momentum at visible wavelengths using a plasmonic metasurface," Light Sci. Appl. **3**, e167 (2014).
22. H. Wang, L. Liu, X. Lu, H. Lv, Y. Han, S. Wang, and S. Teng, "Spatial multiplexing plasmonic metalenses based on nanometer cross holes," New J. Phys. **20**, 123009 (2018).
23. N. Yu and F. Capasso, "Flat optics with designer metasurfaces," Nat. Mater. **13**, 3839 (2014).
24. S. Boroviks, R. A. Deshpande, N. A. Mortensen, and S. I. Bozhevolnyi, "Multifunctional meta-mirror: polarization splitting and focusing," ACS Photon. **5**, 1648–1653 (2017).
25. B. Groever, W. T. Chen, and F. Capasso, "Meta-lens doublet in the visible," Nano Lett. **17**, 4902–4907 (2017).
26. H. Lv, X. Lu, Y. Han, Z. Mou, and S. Teng, "Multifocal metalens with a controllable intensity ratio," Opt. Lett. **44**, 2518–2521 (2019).
27. R. Bao, Z. Mou, C. Zhou, Q. Bai, X. He, Z. Han, S. Wang, and S. Teng, "Generation of diffraction-free beams using resonant metasurfaces," New J. Phys. **22**, 103064 (2020).
28. L. Liu, H. Wang, Y. Han, X. Lu, H. Lv, and S. Teng, "Color filtering and displaying based on hole array," Opt. Commun. **436**, 96–100 (2019).
29. G. Zheng, H. Muhlenbernd, M. Kenney, G. Li, T. Zentgraf, and S. Zhang, "Metasurface holograms reaching 80% efficiency," Nat. Nanotechnol. **10**, 308–312 (2015).
30. L. Huang, X. Chen, H. Mühlenbernd, Z. Hao, S. Chen, B. Bai, Q. Tan, G. Jin, K. W. Cheah, C. W. Qiu, J. Li, T. Zentgraf, and S. Zhang, "Three-dimensional optical holography using a plasmonic metasurface," Nat. Commun. **4**, 2808 (2013).
31. L. Huang, S. Zhang, and T. Zentgraf, "Metasurface holography: from fundamentals to applications," Nanophotonics **7**, 1169–1190 (2018).
32. Z. L. Deng and G. Li, "Metasurface optical holography," Mater. Today Phys. **3**, 16–32 (2017).
33. W. Wan, G. Jie, and X. Yang, "Metasurface holograms for holographic imaging," Adv. Opt. Mater. **5**, 1700541 (2017).
34. Q. Jiang, G. Jin, and L. Cao, "When metasurface meets hologram: principle and advances," Adv. Opt. Photon. **11**, 518–576 (2019).
35. X. Ni, A. V. Kildishev, and V. M. Shalaev, "Metasurface holograms for visible light," Nat. Commun. **4**, 2807 (2013).
36. I. Dolev, I. Epstein, and A. Arie, "Surface-plasmon holographic beam shaping," Phys. Rev. Lett. **109**, 203903 (2012).
37. J. P. Balthasar Mueller, N. A. Rubin, R. C. Devlin, B. Groever, and F. Capasso, "Metasurface polarization optics: independent phase control of arbitrary orthogonal states of polarization," Phys. Rev. Lett. **118**, 113901 (2017).
38. Z. Jin, S. Mei, S. Chen, Y. Li, C. Zhang, Y. He, X. Yu, C. Yu, J. K. W. Yang, B. Luk'yanchuk, and C. W. Qiu, "Complex inverse design of meta-optics by segmented hierarchical evolutionary algorithm," ACS Nano. **13**, 821–829 (2019).
39. L. Jin, Y. W. Huang, Z. Jin, R. C. Devlin, Z. Dong, S. Mei, M. Jiang, W. T. Chen, Z. Wei, H. Liu, J. Teng, A. Danner, X. Li, S. Xiao, S. Zhang, C. Yu, J. K. W. Yang, F. Capasso, and C. W. Qiu, "Dielectric multi-momentum meta-transformer in the visible," Nat. Commun. **10**, 4789 (2019).
40. Z. Mou, X. Lu, H. Lv, Y. Han, and S. Teng, "Metasurface array illuminator based on Fresnel holography," Opt. Lasers Eng. **131**, 106146 (2020).
41. E. Hasman, V. Kleiner, G. Biener, and A. Niv, "Polarization dependent focusing lens by use of quantized Pancharatnam–Berry phase diffractive optics," Appl. Phys. Lett. **82**, 328 (2003).
42. S. Y. Teng, Q. Zhang, H. Wang, L. X. Liu, and H. R. Lv, "Conversion between polarization states based on a metasurface," Photon. Res. **7**, 246–250 (2019).
43. E. D. Palik, *Handbook of Optical Constants of Solids* (Academic, 1985).